This is a repository copy of *High-fidelity initialization of long-lived quantum dot hole spin qubits by reduced fine-structure splitting*.

White Rose Research Online URL for this paper:
http://eprints.whiterose.ac.uk/91609/

Version: Accepted Version

High-fidelity initialization of long-lived quantum dot hole spin qubits by reduced fine-structure splitting

A. J. Brash,[1] L. M. P. P. Martins,[1] F. Liu,[1, *] J. H. Quilter,[1, 2] A. J. Ramsay,[3] M. S. Skolnick,[1] and A. M. Fox[1]

[1] *Department of Physics and Astronomy, University of Sheffield, Sheffield, S3 7RH, United Kingdom*
[2] *Department of Physics, Royal Holloway, University of London, Egham, TW20 0EX, United Kingdom*
[3] *Hitachi Cambridge Laboratory, Hitachi Europe Ltd., Cambridge CB3 0HE, United Kingdom*
(Dated: September 25, 2015)

We demonstrate an on-demand hole spin qubit initialization scheme meeting four key requirements of quantum information processing: fast initialization ($1/e \sim 100$ ps), high fidelity ($F > 99\%$), long qubit lifetime ($2T_h > T_2^* \simeq 10$ ns), and compatibility with optical coherent control schemes. This is achieved by rapidly ionizing an exciton in an InGaAs quantum dot with very low fine-structure splitting at zero magnetic field. Furthermore, we show that the hole spin fidelity of an arbitrary quantum dot can be increased by optical Stark effect tuning of the fine-structure splitting close to zero.

Single hole spins confined in semiconductor quantum dots (QDs) are an attractive stationary qubit candidate owing to their long coherence times[1–3], ultrafast optical coherent control[2–4] and potential for integration with circuit-style devices for quantum information processing (QIP)[5–7]. Initialization of a qubit to a well-defined state is a critical part of any QIP protocol as it limits the fidelity of the entire process. An ideal initialization scheme should be fast, operate on-demand and have high fidelities to permit error correction[8,9], whilst long qubit lifetimes are desirable to maximize the number of possible gate operations.

A range of single carrier spin initialization schemes have previously been demonstrated for both single QDs and quantum dot molecules. These include optical pumping[10–12], coherent population trapping[1,13] and the ionization of an exciton[14–18]. Optical pumping methods have reached fidelities as high as 99.8% in an out-of plane magnetic field[10] with initialization times of the order of μs. Faster (ns) initialization with slightly lower fidelities has been observed in an in-plane magnetic field[11,13]. However, practical fault-tolerant QIP implementations[8,9] require initialization that is very fast compared to decoherence and hence it is desirable to further increase the initialization speed.

When driven by ultrafast pulsed lasers, exciton ionization schemes can offer both picosecond initialization times and on-demand operation. Unfortunately, the anisotropic exchange interaction[19,20] typically reduces fidelity by causing spin precession during the exciton lifetime[16,21,22] [see Fig. 1(b)]. Fast electron tunneling minimizes this effect with fidelities of $F > 96\%$ obtained for ionization in QD molecules[18] and $F > 97\%$ for probabilistic (continuous-wave (CW)) initialization of single QDs[23]. However, a negative consequence is the reduction of the hole qubit's lifetime to 300 ps[18] or 3 ns[23] respectively. This is significantly less than the hole's long extrinsic coherence time ($T_2^* \simeq 10$ ns)[1–4], reducing the coherence time (T_2) and the number of possible gate operations. Application of a strong out-of-plane magnetic field
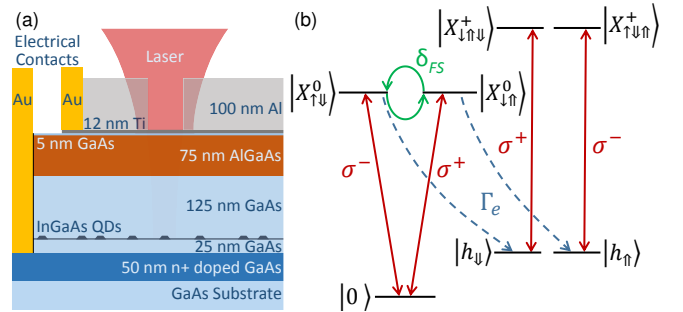

Figure 1. (a) Sample structure. A low density layer of InGaAs QDs is embedded in an n-i-Schottky diode. (b) Energy levels in the circularly polarized basis at zero magnetic field where ($\downarrow$ / $\uparrow$) and ($\Downarrow$ / $\Uparrow$) represent electron and hole spins respectively. The neutral exciton (X^0) states are coupled by the FSS with angular precession frequency δ_{FS} (green arrows) and decay by electron tunneling at a rate Γ_e (blue dashed arrows) to leave single holes (h). The hole spin state can be read out by probing the $h \rightarrow X^+$ (positive trion) transitions using $\sigma^{+/-}$ polarized pulses.

inhibits spin precession resulting in $F > 99\%$[21]; however out of plane fields are incompatible with present coherent control schemes[1–3,24] which require in-plane spin quantization.

In this Rapid Communication we demonstrate $F > 99\%$ at zero magnetic field with on-demand, < 100 ps initialization and a hole lifetime that can be as high as 25.2 ns. This is achieved by exciton ionization in a QD with near-zero fine-structure splitting (FSS), rendering the precession due to the anisotropic exchange interaction negligible relative to the exciton lifetime. To demonstrate that such a scheme is also applicable to typical QDs with finite FSS, we use the optical Stark effect (OSE)[25] to reduce the FSS[26,27], resulting in increased fidelity.

The sample consists of InGaAs/GaAs self-assembled QDs embedded in the intrinsic region of an n-i-Schottky diode [see Fig. 1(a)]. Five QDs with FSS ranging from
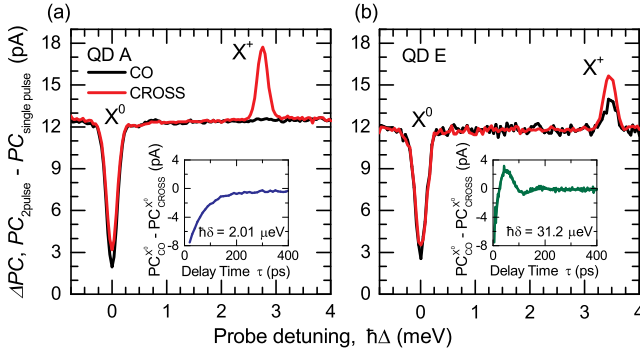
Figure 2. Two-color pump-probe photocurrent spectra of quantum dots exhibiting (a) negligible (2.01 µeV) and (b) large (31.2 µeV) FSS. Spectra are measured at $E = 72$ kV cm^{-1} and $\tau = 100$ ps when only the hole is left in the QD. Black (red) lines correspond to a co (cross)-polarized probe laser. Insets: The precession of the neutral exciton spin measured by time-resolved pump-probe spectroscopy[31]. The exponential damping of the fine-structure beats corresponds to the exciton lifetime ($1/\Gamma_X$).
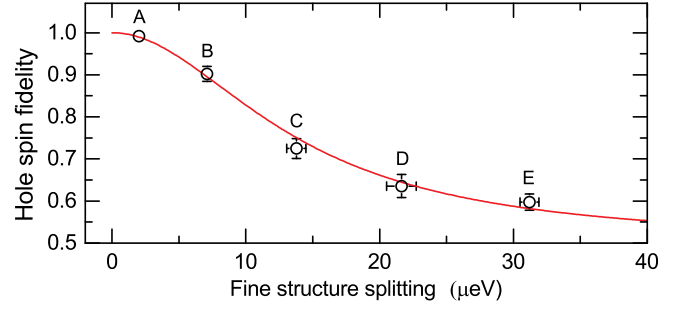

Figure 3. Fidelity vs. fine-structure splitting as measured for QDs with different FSS. For all QDs, F was measured at $\Gamma_e = 0.021 \, \text{ps}^{-1}$. The red line is a calculation using Eq. 2.

2.01 µeV (QD A) to 31.2 µeV (QD E) were studied. The sample is held in a helium bath cryostat at 4.2 K and excited by transform-limited FWHM $\simeq 0.2$ meV pulses derived from a Ti:Sapphire laser with 76 MHz repetition rate. Photoexcited carriers in the QD are then detected by measuring the resulting photocurrent[28].

Figure 1(b) illustrates the principle of the hole spin initialization scheme. A circularly-polarized laser pulse with π pulse area creates a neutral exciton (X^0) in the QD at time $t = 0$. Under a reverse bias DC electric field (E) the exciton population decays at a rate $\Gamma_X = \Gamma_r + \Gamma_e + \Gamma_h$ where Γ_r is the rate of radiative recombination and Γ_e and Γ_h are the electron and hole tunneling rates respectively. Owing to the larger hole effective mass the electron tunneling rates exceed hole tunneling rates by around two orders of magnitude ($\Gamma_e \gg \Gamma_h$). Radiative recombination rates are slow compared to electron tunneling in our devices[29,30] and hence $\Gamma_X \simeq \Gamma_e$. The tunneling of the electron leaves behind a single hole with spin conserved from the X^0; thus the initialization time for the hole is equal to $1/\Gamma_e$. The anisotropic exchange interaction causes precession between $X^0_{\uparrow\Downarrow}$ and $X^0_{\downarrow\Uparrow}$ states at angular frequency δ_{FS}, reducing the polarization of the resultant hole spin.

To measure the initialized hole spin, a co (cross)-circularly polarized probe π pulse arrives after a delay (τ) with a detuning of Δ relative to the first pulse. By scanning the probe detuning, two-pulse spectra like those shown in Fig. 2 are obtained where black (red) traces represent the co (cross)-polarized cases respectively. For presentation purposes, a single-pulse (probe only) spectrum is subtracted from the two-pulse spectrum to remove any weak spectral features not arising from the pumped QD; the dip at $\Delta = 0$ corresponds to subtraction of the X^0 peak. At Δ equal to the positive trion

(X^+) binding energy the $h \rightarrow X^+$ transitions shown in Fig. 1(b) are probed. Peaks corresponding to these transitions are observed in the spectra and the hole spin state may be extracted from their relative amplitudes.

Figure 2(a) shows the spectrum of QD A with a small FSS of 2.01 µeV. The inset illustrates that exciton spin precession during electron tunneling is negligible; as a result, the hole spin preparation is almost ideal with no trion peak observed for a co-polarized probe. By contrast, Fig. 2(b) shows the case of QD E with a large FSS of 31.2 µeV. The exciton spin precession is seen clearly in the inset whilst prominent trion peaks in both spectra illustrate the reduced fidelity.

The fidelity[32] of spin preparation is defined as $F = \langle \Uparrow | \rho | \Uparrow \rangle$ where ρ is the density matrix of the prepared spin state and $\Uparrow$ ($\Downarrow$) is the target spin state. Fidelity is evaluated using Eq. 1:

$$F = \frac{PC^{X^+}_{\text{cross}}}{PC^{X^+}_{\text{cross}} + PC^{X^+}_{\text{co}}}, \tag{1}$$

where $PC^{X^+}_{cross}$ and $PC^{X^+}_{co}$ are the amplitudes of the X^+ peaks in the co- and cross-polarized spectra.

To investigate the variation of F with δ_{FS}, the fidelities of the five QDs with different FSS are measured at a constant electron tunneling rate (Γ_e) by varying the DC electric field. The tunneling rates and FSS are measured by time-resolved pump-probe spectroscopy[31,33] whilst the smallest FSS are measured with a narrow linewidth (FWHM < 10 neV) CW laser [see Ref. 34]. The data is shown in Fig. 3 where F falls as the fine-structure precession increases relative to electron tunneling. At $B = 0$ T, the hole spin fidelity is described by a model developed by Godden et al.[21]:

$$F = 1 - \frac{1}{2} \left[\frac{\delta^2_{FS}}{\delta^2_{FS} + (\Gamma_X - \Gamma_h)^2} \right], \tag{2}$$

where $(\Gamma_X - \Gamma_h) \simeq \Gamma_e$ due to slow radiative recombination as previously discussed.. The line in Fig. 3 shows a calculation of F using Eq. 2, demonstrating a
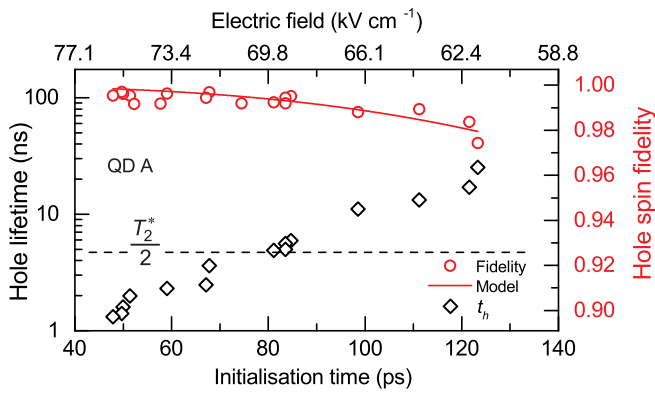
Figure 4. Hole lifetime ($1/\Gamma_h$) (diamonds) and fidelity lower bound (red circles) plotted vs. initialization time ($1/\Gamma_e$) and approximate DC electric field for QD A. Error bars are of the order of the data point size. The model (red line) represents a fit of Eq. 2 with measured $\hbar\delta_{FS} = 2.01 \pm 0.20\,\mu eV$ and fitting parameter $\hbar\chi_E = -0.0219 \pm 0.0007\,\mu eV\,V^{-1}\,cm$ corresponding to a small change in FSS with DC electric field [see Ref. 34].

good quantitative agreement with our results. For QD A ($\hbar\delta_{FS} = 2.01 \pm 0.20$ μeV) a fidelity lower bound of $F \geq 0.993$ is measured. This value is only limited by the noise present in the co-polarized spectrum and implies an initialization error rate below the 0.75% threshold required for error correction[43].

Owing to the negligible exciton spin precession of QD A, fast electron tunneling is no longer required to achieve high fidelities. This enables the reduction of the diode electric field to maximize the hole lifetime ($T_h = 1/\Gamma_h$) with a moderate increase in initialization time ($1/\Gamma_e$ which remains $\ll$ than the coherence time (T_2)) and a small change in FSS[41]. Previous studies on similar samples have shown that the coherence time of the hole spin is limited by the hole tunneling rate[3] (Γ_h) at typical electric fields. Beyond this, the next limit is the extrinsic pure dephasing time ($T_2^* \simeq 10$ ns[1–4]) which most likely originates from fluctuations in the electric field acting on the hole g-factor[2,4,44]. In the limit of negligible extrinsic pure dephasing, or spin-flips, the coherence time is twice the hole lifetime. Thus, a good target is $2T_h > T_2^*$, the point at which pure dephasing rather than hole tunneling becomes the dominant limitation on the coherence time.

To demonstrate this, Fig. 4 shows the results of measuring fidelity, initialization time and hole lifetime for a range of DC electric fields on the low FSS QD A. By treating the variation of δ_{FS} with DC electric field as a fitting parameter in Eq. 2 [see Ref. 34] we obtain excellent agreement with the data [see red line]. At lower electric fields the maximum resolvable fidelity decreases due to reduced photocurrent, emphasizing that our measurements represent a lower-bound. For $2T_h > T_2^*$ the initialization time ranges from 83.5 ps to 123 ps with fidelity lower bounds from ≥ 0.974 to ≥ 0.995, indicating that both high fidelity and long qubit lifetimes may be obtained for a QD with negligible FSS.

Due to the importance of low FSS QDs for polarization entangled photon sources[45,46], deterministic growth of symmetric QDs is a topical area of research[47–49] but is yet to be demonstrated. As such, in-situ methods for tuning FSS are widely studied, using strain[50,51], magnetic[52] and laser[26,27] fields as well as both lateral[53,54] and vertical[55,56] DC electric fields. In order to retain control over the qubit energy and lifetime it is desirable to tune the FSS using a field that is independent from the DC electric field. Thus we use a detuned CW laser to tune δ_{FS} by the OSE[25–27] at a fixed DC electric field.

In our scheme the OSE is induced by a linearly polarized CW laser which is positively detuned from the co-polarized $X \to XX$ (biexciton) transition by Δ_{CW} as illustrated in Fig. 5(a). The neutral exciton eigenstates ($X_{H/V}$) are linearly polarized along the in-plane crystal axes and can be addressed individually by selecting the laser polarization. X_H and X_V are split by $\hbar\delta_{FS}$; we define X_V to be lower in energy. A positive-detuned V-polarized laser addresses the X_V state and acts to reduce δ_{FS} by Stark-shifting the X_V state to higher energy. By contrast, an H-polarized laser increases δ_{FS} by shifting the X_H state to higher energy. In the case of positive detuning ($\Delta_{CW} > 0$), the change in FSS due to the OSE ($\Delta\omega$) is given by[25]:

$$\Delta\omega = \frac{s}{2}\left(\Delta_{CW} - \sqrt{\Delta_{CW}^2 + |\Omega|^2}\right) \qquad (3)$$

where Ω is the Rabi splitting induced by the CW laser (proportional to the square-root of laser intensity $\sqrt{I}$) and $s = \pm 1$ when the CW laser is H/V polarized. Similar to previous reports[26,42], we observe a polarization-independent blue-shift of the exciton energy with I. This arises due to charge screening from the large number of carriers generated in the surrounding material by the CW laser and results in a linear dependence of Δ_{CW} on I.

In Fig. 5(b) the CW laser photon energy is fixed and the FSS of QD C is measured by time-resolved pump-probe spectroscopy [as in insets to Fig. 2] as a function of both laser intensity (I) and polarization. For a V-polarized CW laser (red circles), δ_{FS} reduces from its initial value of $\hbar\delta_{FS} = 13.2 \pm 0.1$ μeV to a minimum of $\hbar\delta_{FS} = 2.49 \pm 1.25$ μeV at $I = 0.44$ kW cm^{-2}. Conversely, when the laser is H-polarized (blue diamonds) δ_{FS} increases, proving that the change in FSS is induced by the OSE. The solid lines show a fit of Eq. 3 to the data [see Ref. 34].

To demonstrate that reducing FSS leads to an increase in fidelity, hole spin fidelity was measured as a function of CW laser intensity. The laser is V-polarized and $\hbar\Delta_{CW} = 33.4$ μeV. The result of this measurement is shown in Fig. 5(c); for $I = 0.25$ kW cm^{-2} (FSS $\simeq 8.7$ μeV) a fidelity of $F = 0.868 \pm 0.036$ is measured, an increase of 0.142 over that measured with no CW laser. The red line shows a calculation using Eq. 2 with experimentally derived parameters [see details in Ref. 34] which again agrees closely with the data. In both experiments, the
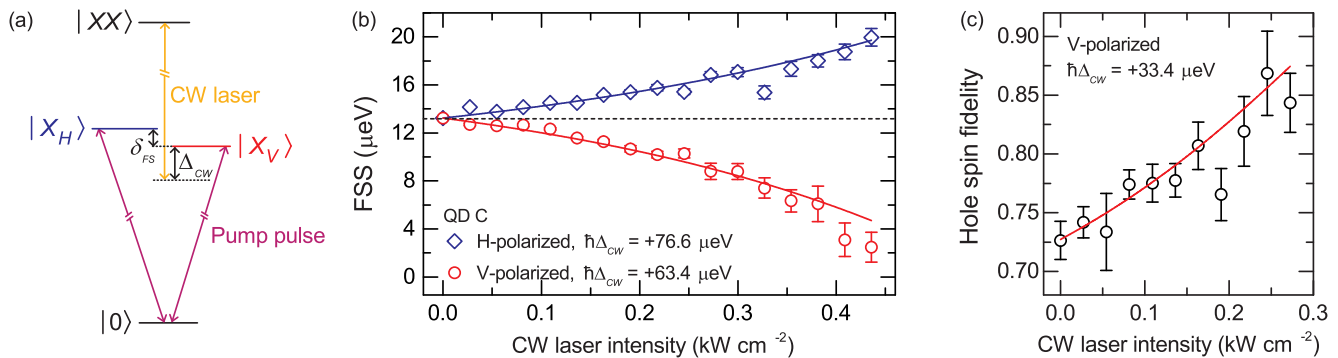
Figure 5. (a) QD energy levels in the linear basis where the neutral exciton eigenstates are split by δ_{FS}. The CW laser is V-polarized and positively detuned from the $X_V \to XX$ transition by $\triangle_{CW}$. The pump pulse addresses both exciton levels owing to its circular polarization and FWHM $\gg \delta_{FS}$. (b) FSS vs. CW laser intensity for QD C with $\hbar\delta_{FS} = 13.2\,\mu\text{eV}$ measured at $E = 60$ kV cm^{-1} to resolve small δ_{FS}. The blue diamonds (red circles) correspond to an H (V)-polarized CW laser which addresses the high (low) energy exciton eigenstate. The solid lines are fits to Eq. 3. (c) Hole spin fidelity (measured as in Fig. 2) vs. CW laser intensity for a V-polarized CW laser at $E = 72$ kV cm^{-1} to maximize photocurrent detection efficiency. The line is a fit of the model (Eq. 2) incorporating the variation of δ_{FS} with CW laser intensity [see Ref. 34] .

maximum I is limited by photocurrent fluctuations due to laser power instability. This particularly limits the fidelity measurement as at $I > 0.25\,\text{kW cm}^{-2}$ fluctuations exceed the small (~ 1 pA) co-polarized peak amplitude, limiting the maximum F that can be measured. However, the agreement with the model and the large optical Stark shift observed in Fig. 5(b) indicate that fidelities as high as those measured for QD A could in principle be obtained with this method. We also note that the anti-crossing behavior seen with tuning methods such as strain[57] does not occur for the OSE[26].

In conclusion, we have demonstrated that a QD with very small FSS ($2.01 \pm 0.20\,\mu\text{eV}$) enables fast, on-demand initialization of a long-lived ($2T_h > T_2^* \sim 10$ ns) hole spin qubit with fidelity $\geq 99.5\%$ at $B = 0$ T, exceeding the threshold required for a fault-tolerant QIP implementation[43]. Whilst the high fidelities here are measured at zero magnetic field, we note that simulations with small δ_{FS} show that F will remain very high even under the presence of a modest in-plane magnetic field[22]. As a result, this initialization scheme offers performance compatible with coherent control of hole spins[1–3,24] where fast gate times ($\sim$20 ps[2,3]), high gate fidelities (94.5%[2]) and long coherence lifetimes have demonstrated an attractive qubit platform. We note that hole lifetimes could be further extended by modulation of the electric field to a very low value between initialization and readout[58]. Combining this with supression of extrinsic pure dephasing by optical spin echo[59] could enable high fidelity initialization with coherence times in the μs regime.

Furthermore, we have demonstrated that the initialization fidelity for arbitrary QDs with larger FSS can be increased by the OSE, providing additional motivation for FSS tuning studies[26,27,50–56] that were typically motivated by the generation of entangled photon pairs[45,46]. In our devices the DC electric field presents an extra tunable parameter that may be used to optimize qubit lifetimes [see Fig. 4] or to tune two QDs into resonance. This presents a potential route towards fault-tolerant QIP schemes based on multiple long-lived hole spins on a single chip.

Note added in proof. Recently, we became aware of related results by another group[60].

ACKNOWLEDGMENTS

* To whom correspondence should be addressed: FengLiu@sheffield.ac.uk

[1] D. Brunner, B. D. Gerardot, P. A. Dalgarno, G. Wüst, K. Karrai, N. G. Stoltz, P. M. Petroff, and R. J. Warburton, Science **325**, 70 (2009).

[2] K. De Greve, P. L. McMahon, D. Press, T. D. Ladd, D. Bisping, C. Schneider, M. Kamp, L. Worschech, S. Hofling, A. Forchel, and Y. Yamamoto, Nat Phys **7**, 872 (2011).

[3] T. M. Godden, J. H. Quilter, A. J. Ramsay, Y. Wu, P. Brereton, S. J. Boyle, I. J. Luxmoore, J. Puebla-Nunez, A. M. Fox, and M. S. Skolnick, Phys. Rev. Lett. **108**, 017402 (2012).

[4] A. Greilich, S. G. Carter, D. Kim, A. S. Bracker, and D. Gammon, Nat Photon **5**, 702 (2011).

[5] W. B. Gao, P. Fallahi, E. Togan, J. Miguel-Sanchez, and

A. Imamoglu, Nature **491**, 426 (2012).

[6] K. De Greve, L. Yu, P. L. McMahon, J. S. Pelc, C. M. Natarajan, N. Y. Kim, E. Abe, S. Maier, C. Schneider, M. Kamp, S. Hofling, R. H. Hadfield, A. Forchel, M. M. Fejer, and Y. Yamamoto, Nature **491**, 421 (2012).

[7] N. Prtljaga, R. J. Coles, J. O'Hara, B. Royall, E. Clarke, A. M. Fox, and M. S. Skolnick, Applied Physics Letters **104**, 231107 (2014).

[8] D. P. DiVincenzo, Fortschritte der Physik **48**, 771 (2000).

[9] J. Preskill, Proceedings of the Royal Society A: Mathematical, Physical and Engineering Sciences **454**, 385 (1998).

[10] M. Atatüre, J. Dreiser, A. Badolato, A. Högele, K. Karrai, and A. Imamoglu, Science **312**, 551 (2006).

[11] X. Xu, Y. Wu, B. Sun, Q. Huang, J. Cheng, D. G. Steel, A. S. Bracker, D. Gammon, C. Emary, and L. J. Sham, Phys. Rev. Lett. **99**, 097401 (2007).

[12] D. Kim, S. E. Economou, S. C. Badescu, M. Scheibner, A. S. Bracker, M. Bashkansky, T. L. Reinecke, and D. Gammon, Phys. Rev. Lett. **101**, 236804 (2008).

[13] X. Xu, B. Sun, P. R. Berman, D. G. Steel, A. S. Bracker, D. Gammon, and L. J. Sham, Nat Phys **4**, 692 (2008).

[14] M. Kroutvar, Y. Ducommun, D. Heiss, M. Bichler, D. Schuh, G. Abstreiter, and J. J. Finley, Nature **432**, 81 (2004).

[15] R. J. Young, S. J. Dewhurst, R. M. Stevenson, P. Atkinson, A. J. Bennett, M. B. Ward, K. Cooper, D. A. Ritchie, and A. J. Shields, New Journal of Physics **9**, 365 (2007).

[16] A. J. Ramsay, S. J. Boyle, R. S. Kolodka, J. B. B. Oliveira, J. Skiba-Szymanska, H. Y. Liu, M. Hopkinson, A. M. Fox, and M. S. Skolnick, Phys. Rev. Lett. **100**, 197401 (2008).

[17] D. Heiss, V. Jovanov, M. Bichler, G. Abstreiter, and J. J. Finley, Phys. Rev. B **77**, 235442 (2008).

[18] K. Müller, A. Bechtold, C. Ruppert, C. Hautmann, J. S. Wildmann, T. Kaldewey, M. Bichler, H. J. Krenner, G. Abstreiter, M. Betz, and J. J. Finley, Phys. Rev. B **85**, 241306 (2012).

[19] D. Gammon, E. S. Snow, B. V. Shanabrook, D. S. Katzer, and D. Park, Physical Review Letters **76**, 3005 (1996).

[20] M. Bayer, G. Ortner, O. Stern, A. Kuther, A. Gorbunov, A. Forchel, P. Hawrylak, S. Fafard, K. Hinzer, T. Reinecke, S. Walck, J. Reithmaier, F. Klopf, and F. Schäfer, Physical Review B **65**, 195315 (2002).

[21] T. M. Godden, S. J. Boyle, A. J. Ramsay, A. M. Fox, and M. S. Skolnick, Applied Physics Letters **97**, 061113 (2010).

[22] T. M. Godden, J. H. Quilter, A. J. Ramsay, Y. Wu, P. Brereton, I. J. Luxmoore, J. Puebla, A. M. Fox, and M. S. Skolnick, Phys. Rev. B **85**, 155310 (2012).

[23] J. D. Mar, J. J. Baumberg, X. Xu, A. C. Irvine, and D. A. Williams, Phys. Rev. B **90**, 241303 (2014).

[24] J. Hansom, C. H. H. Schulte, C. Le Gall, C. Matthiesen, E. Clarke, M. Hugues, J. M. Taylor, and M. Atature, Nat Phys **10**, 725 (2014).

[25] T. Unold, K. Mueller, C. Lienau, T. Elsaesser, and A. D. Wieck, Phys. Rev. Lett. **92**, 157401 (2004).

[26] G. Jundt, L. Robledo, A. Högele, S. Fält, and A. Imamoglu, Phys. Rev. Lett. **100**, 177401 (2008).

[27] A. Muller, W. Fang, J. Lawall, and G. S. Solomon, Phys. Rev. Lett. **103**, 217402 (2009).

[28] A. Zrenner, E. Beham, S. Stufler, F. Findeis, M. Bichler, and G. Abstreiter, Nature **418**, 612 (2002).

[29] W. Langbein, P. Borri, U. Woggon, V. Stavarache, D. Reuter, and A. D. Wieck, Phys. Rev. B **70**, 033301 (2004).

[30] P. A. Dalgarno, J. M. Smith, J. McFarlane, B. D. Gerardot, K. Karrai, A. Badolato, P. M. Petroff, and R. J. Warburton, Phys. Rev. B **77**, 245311 (2008).

[31] A. F. A. Khatab, A. J. Ramsay, S. J. Boyle, A. M. Fox, and M. S. Skolnick, Journal of Physics: Conference Series **245**, 012010 (2010).

[32] R. Jozsa, Journal of Modern Optics **41**, 2315 (1994).

[33] R. S. Kolodka, A. J. Ramsay, J. Skiba-Szymanska, P. W. Fry, H. Y. Liu, A. M. Fox, and M. S. Skolnick, Phys. Rev. B **75**, 193306 (2007).

[34] See Supplemental Material (which follows the manuscript) for further details of the measurement techniques and the models used, which includes Refs. [21, 23, 24, 27, 29, 31-38].

[35] T. M. Godden, *Coherent optical control of the spin of a single hole in a quantum dot*, Ph.D. thesis, University of Sheffield (2012).

[36] J. H. Quilter, *Coherent spectroscopy of single quantum dots*, Ph.D. thesis, University of Sheffield (2014).

[37] P. W. Fry, I. E. Itskevich, S. R. Parnell, J. J. Finley, L. R. Wilson, K. L. Schumacher, D. J. Mowbray, M. S. Skolnick, M. Al-Khafaji, A. G. Cullis, M. Hopkinson, J. C. Clark, and G. Hill, Physical Review B **62**, 16784 (2000).

[38] S. Stufler, P. Ester, A. Zrenner, and M. Bichler, Applied Physics Letters **85**, 4202 (2004).

[39] P. Ester, S. Stufler, S. Michaelis de Vasconcellos, M. Bichler, and A. Zrenner, Physica Status Solidi (c) **3**, 3722 (2006).

[40] J. Houel, A. V. Kuhlmann, L. Greuter, F. Xue, M. Poggio, B. D. Gerardot, P. A. Dalgarno, A. Badolato, P. M. Petroff, A. Ludwig, D. Reuter, A. D. Wieck, and R. J. Warburton, Phys. Rev. Lett. **108**, 107401 (2012).

[41] E. Kadantsev and P. Hawrylak, Phys. Rev. B **81**, 045311 (2010).

[42] X. Xu, B. Sun, P. R. Berman, D. G. Steel, A. S. Bracker, D. Gammon, and L. J. Sham, Science **317**, 929 (2007).

[43] R. Raussendorf and J. Harrington, Phys. Rev. Lett. **98**, 190504 (2007).

[44] A. V. Kuhlmann, J. Houel, A. Ludwig, L. Greuter, D. Reuter, A. D. Wieck, M. Poggio, and R. J. Warburton, Nat Phys **9**, 570 (2013).

[45] R. M. Stevenson, R. J. Young, P. Atkinson, K. Cooper, D. a. Ritchie, and a. J. Shields, Nature **439**, 179 (2006).

[46] N. Akopian, N. H. Lindner, E. Poem, Y. Berlatzky, J. Avron, D. Gershoni, B. D. Gerardot, and P. M. Petroff, Physical Review Letters **96**, 130501 (2006), 0512048v2 [arXiv:quant-ph].

[47] J. Treu, C. Schneider, A. Huggenberger, T. Braun, S. Reitzenstein, S. Höfling, and M. Kamp, Applied Physics Letters **101**, 022102 (2012).

[48] G. Juska, V. Dimastrodonato, L. O. Mereni, A. Gocalinska, and E. Pelucchi, Nat Photon **7**, 527 (2013).

[49] Y. H. Huo, A. Rastelli, and O. G. Schmidt, Applied Physics Letters **102**, 152105 (2013).

[50] S. Seidl, M. Kroner, A. Högele, K. Karrai, R. J. Warburton, A. Badolato, and P. M. Petroff, Applied Physics Letters **88**, 203113 (2006).

[51] R. Trotta, E. Zallo, C. Ortix, P. Atkinson, J. D. Plumhof, J. van den Brink, A. Rastelli, and O. G. Schmidt, Phys. Rev. Lett. **109**, 147401 (2012).

[52] R. M. Stevenson, R. J. Young, P. See, D. G. Gevaux, K. Cooper, P. Atkinson, I. Farrer, D. A. Ritchie, and A. J. Shields, Phys. Rev. B **73**, 033306 (2006).

[53] K. Kowalik, O. Krebs, A. Lemaitre, B. Eble, A. Kudelski, P. Voisin, S. Seidl, and J. A. Gaj, Applied Physics Letters

91, 183104 (2007).

[54] B. D. Gerardot, S. Seidl, P. A. Dalgarno, R. J. Warburton, D. Granados, J. M. Garcia, K. Kowalik, O. Krebs, K. Karrai, A. Badolato, and P. M. Petroff, Applied Physics Letters **90**, 041101 (2007).

[55] A. J. Bennett, M. A. Pooley, R. M. Stevenson, M. B. Ward, R. B. Patel, A. B. de la Giroday, N. Skold, I. Farrer, C. A. Nicoll, D. A. Ritchie, and A. J. Shields, Nat Phys **6**, 947 (2010).

[56] M. Ghali, K. Ohtani, Y. Ohno, and H. Ohno, Nat Commun **3**, 661 (2012).

[57] J. D. Plumhof, V. Křápek, F. Ding, K. D. Jöns, R. Hafenbrak, P. Klenovský, A. Herklotz, K. Dörr, P. Michler, A. Rastelli, and O. G. Schmidt, Phys. Rev. B **83**, 121302 (2011).

[58] J. H. Quilter, R. J. Coles, A. J. Ramsay, A. M. Fox, and M. S. Skolnick, Applied Physics Letters **102**, 181108 (2013).

[59] D. Press, K. De Greve, P. L. McMahon, T. D. Ladd, B. Friess, C. Schneider, M. Kamp, S. Hofling, A. Forchel, and Y. Yamamoto, Nat Photon **4**, 367 (2010).

[60] P.-L. Ardelt, T. Simmet, K. Müller, C. Dory, K. A. Fischer, A. Bechtold, A. Kleinkauf, H. Riedl, and J. J. Finley, Phys. Rev. B **92**, 115306 (2015).

Supplemental Materials: High-fidelity initialization of long-lived quantum dot hole spin qubits by reduced fine-structure splitting

1. Measurements of fidelity

Fidelity is measured according to Eq. 2 in the body of the paper. For very high fidelities, it is no longer reliable or meaningful to fit a Gaussian peak to the co-polarized spectrum. In this case we use the variance of the photocurrent noise to estimate the amplitude[35] and report a lower bound. We sample the datapoints within the laser FWHM of the trion energy and then calculate the amplitude estimate (ϵ) as in Eq. S1:

$$\epsilon = \frac{\sigma}{\sqrt{N}}, \tag{S1}$$

where N is the number of datapoints within the sample and σ is their standard deviation. The quantity ϵ then replaces $PC_{co}^{X^+}$ in Eq. 2 to calculate the lower bound of F.

2. Conversion of biased voltage to DC electric field

The application of a reversed biased voltage (V) generates a direct current (DC) electric field (E) inside the diode structure. The voltage can be converted to electric field accroding to[36]:

$$E = (V + V_{bi})/W_i, \tag{S2}$$

where V_{bi} (~ 0.76 V) is the built-in voltage of the diode. W_i (230 nm) is the distance between the Ohmic and Schottky contacts.

3. Measurement of small FSS

In order to measure small FSS we use a narrow linewidth CW laser (FWHM ~ 1 MHz) operating at a fixed wavelength to perform high resolution photocurrent spectroscopy[37–39]. The $0 \rightarrow X$ transition is Stark-shifted through the laser line by changing the applied DC electric field. After conversion from DC electric field to energy, the result is a Lorentzian lineshape with typical linewidth $\sim 40\,\mu$eV as illustrated in Fig. S1. The linewidth broadening relative to the exciton decay time limit of ($\sim 14\,\mu$eV determined by the electron tunnelling rate) is attributed to charge fluctuations in the electrostatic environment of the dot during the measurement[40].
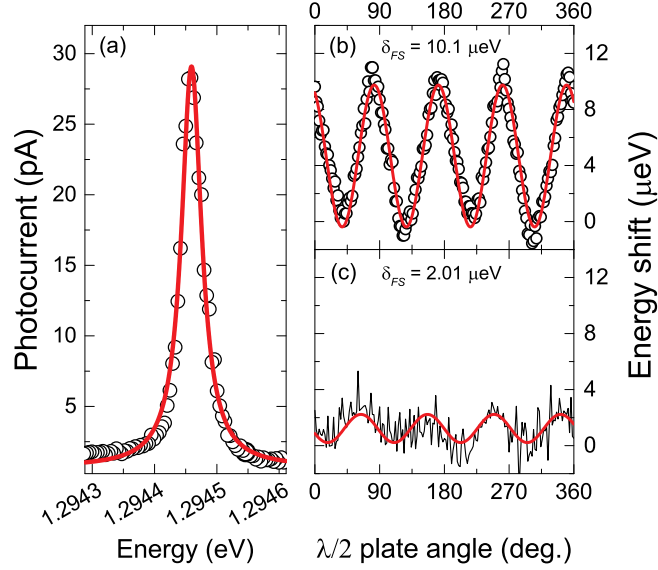
Figure S1. (a) Typical high-resolution photocurrent spectrum of a QD with Lorentzian fit (red line) of linewidth FWHM = $39.3 \pm 0.3\,\mu$eV. Plot of the neutral exciton energy of QDs with (b) moderate δ_{FS} and (c) very small δ_{FS} (QD A) as a function of half-wave plate angle. Red lines: Fitting with $\sin^2(\theta)$ function. The amplitude of the fits yields a fine structure splitting of $\hbar\delta_{FS} = 10.1 \pm 0.1\,\mu$eV and $2.01 \pm 0.2\,\mu$eV respectively.

Rotating the linear polarization angle of the CW laser with a half-wave plate causes the exciton energy to oscillate with an amplitude of $\hbar\delta_{FS}$ as illustrated for a QD with moderate δ_{FS} ($10.1 \pm 0.1\,\mu$eV) and very small δ_{FS} ($2.01 \pm 0.20\,\mu$eV) (QD A) in Fig. S1(b) and (c).

4. Model of fidelity vs. applied DC electric field

The key modification to the model of Eq. 1 for experiments at non-constant DC electric field [see Fig. 4 in the main paper] is to consider the variation of FSS with DC electric field[41]. In this case the expression for FSS is defined by Eq. S3:

$$\delta_{FS}(E) = \delta_{FS}\big|_{E_0} + \chi_E[E - E_0], \tag{S3}$$

where $\delta_{FS}\big|_{E_0}$ is the FSS evaluated at E_0 and χ_E is a linear gradient of FSS with E. The linear gradient represents a good approximation of the form of χ_E however full calculations require numerical methods[41]. For larger FSS we can simply measure $\hbar\chi_E$ [as shown in Fig. S2] using time-resolved pump-probe measurements [as shown in the insets to Fig. 2 of the main paper] . The fittings give $\hbar\chi_E = 0.25 \pm 0.04\,\mu$eV V^{-1} cm for QD E and $-0.10 \pm 0.02\,\mu$eV V^{-1} cm for QD C. These values are consistent with the literature value ($0.285\,\mu$eV V^{-1} cm) reported by Bennett et al.[34] and align with the theoretical prediction that smaller values of δ_{FS} (i.e. initial QD anisotropy) give smaller values of χ_E[41].

As such, we expect a very small value of $\hbar\chi_E$ for QD A ($\hbar\delta_{FS} = 2.01 \pm 0.20\,\mu$eV). Since the FSS of QD A is already more than an order of magnitude smaller than the QD linewidth [see Fig. S1], χ_E is used as a fitting parameter. Inserting Eq. S3 into the model of Godden et al.[21] [Eq. 2 in the main text] and fitting χ_E produces the line shown in Fig. 4 of the paper. The extracted value of $\hbar\chi_E = -0.0219 \pm 0.0007\,\mu$eV V^{-1} cm is physically reasonable and again agrees with the expected trend between δ_{FS} and χ_E.

5. Fine structure splitting vs. CW laser intensity

To demonstrate the tuning of δ_{FS} using OSE, we measured the FSS of dot C by time-resolved pump-probe[31] with an additional tuneable narrowband CW laser incident on the sample. The CW laser which is H/V-polarized and positively deutned from the $X \rightarrow XX$ transition [see Fig. 5(a) in the main paper] is used to tune the FSS. Fig. S3
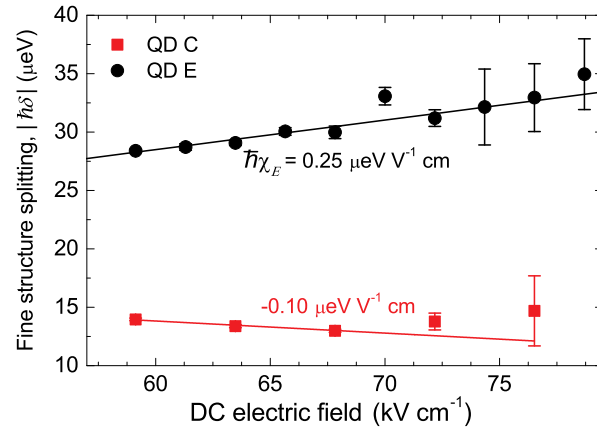
Figure S2. Variation of FSS with DC electric field for QDs C and E with different values of δ_{FS}. The labels show the values of $\hbar\chi_E$ extracted from the linear fits. The opposite signs result from the two QDs being elongated along orthogonal crystal axes whilst the deviation of the red data points from the fit at high DC electric field corresponds to the onset of $\Gamma_X \gg \delta_{FS}$ and thus the resolution limit for a given QD and DC electric field. This figure is adapted from Ref.[36].
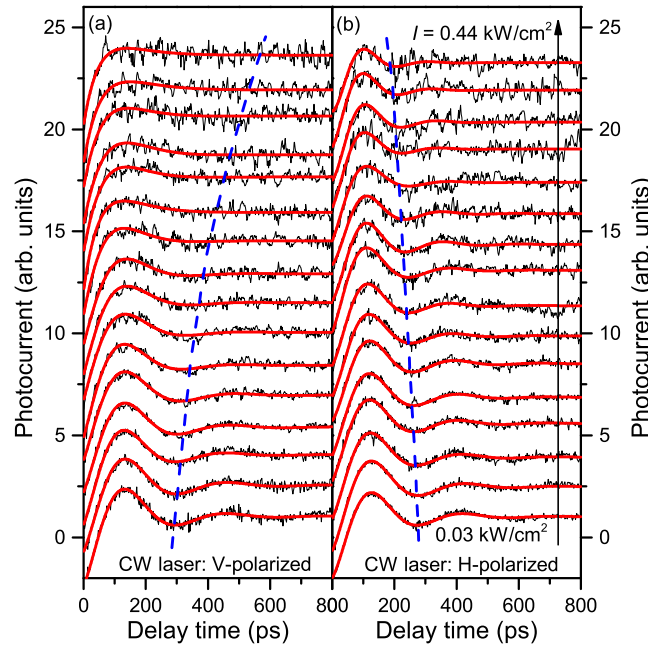

Figure S3. Fine structure precession of the exciton spin vs. CW laser intensity I measured by time-resolved pump-probe photocurrent technique. The CW laser is either (a) V- or (b) H-polarized and positively detuned from the $X \rightarrow XX$ transition (see Fig. 5(a) in the main paper). Detuning = 76.6 and 63.4 μeV when the CW laser is H/V-polarized respectively. The CW laser intensity ranges from 0.03 to 0.44 kW/cm^2. Red lines: Fitting with an exponentially damped sine function. Blue lines: guides for the eye.

shows the fine structure precession of the exciton spin vs. the CW laser intensity I. Since the smallest δ_{FS} that can be resolved by this measurement is limited by the exciton decay time, a relatively low DC electric field ($E = 60$ kV cm^{-1}) was used. When the CW laser is V-polarized [see Fig. S3(a)], the frequency of the fine structure precession decreases with the CW laser intensity. At $I = 0.44$ kW cm^{-2}, no fine structure precession is observed, indicating that a very small FSS close to the resolution limit of the time-resolved pump-probe measurement is achieved. By contrast, the frequency of the fine structure precession increases with CW laser intensity when the CW laser is H-polarized [see Fig. S3(b)], verifying that the change of the FSS is induced by OSE. δ_{FS} can be extracted by fitting the data with an exponentially damped sine function [see red lines]. The δ_{FS} vs. the CW laser intensity is shown in Fig. 5(b) in the main paper.

Polarization	$\hbar\delta_{FS}\vert_{I=0}$(μeV)	s	a (meV^{2}μm^2 W^{-1})	$\hbar\triangle_{CW}\vert_{I=0}$ (μeV)	k (eV μm^2 W^{-1})
H	13.2	$+1$	275	76.6	8.4
V	13.2	-1	275	63.4	8.4

Table S1. Parameters used in the fits of FSS vs. CW laser power [see Fig. 5(b) in the main paper].

Polarization	$\hbar\delta_{FS}\vert_{I=0}$(μeV)	s	a (meV^{2}μm^2 W^{-1})	$\hbar\triangle_{CW}\vert_{I=0}$ (μeV)	k (eV μm^2 W^{-1})	$\Gamma_X - \Gamma_h$(ps^{-1})
V	13.2	-1	275	33.4	3.5	0.021

Table S2. Parameters used in the fit of hole spin fidelity vs. CW laser power [see Fig. 5(c) in the main paper].

6. Model of fidelity vs. OSE

The increase of the hole spin fidelity by reducing the FSS using OSE [see Fig. 5(c) in the main paper] can be well described by incorporting the OSE into the model of Godden et al.[21] (see Eq. 2 in the main text). The FSS with the presence of a CW laser postivltiy detuend from the $X \to XX$ transition [see Fig. 5(a) in the main paper] is given by:

$$\delta_{FS}(I) = \delta_{FS}\vert_{I=0} + \Delta\omega, \tag{S4}$$

$$\Delta\omega = \frac{s}{2}\left(\Delta_{CW} - \sqrt{\Delta_{CW}^2 + |\Omega|^2}\right), \tag{S5}$$

where I is the CW laser intensity. $\Delta\omega$ is the change of the FSS induced by OSE[25]. Δ_{CW} is the detuning of the CW laser. $s = \pm 1$ when the CW laser is H/V polarized. $\Omega = \sqrt{aI}/\hbar$ is the Rabi splitting induced by the CW laser. a is a fitting parameter proportional to the optical dipole momentum of the $X \to XX$ transition. In these experiments a linear blue-shift of the $0 \to X_{H/V}$ transitions with laser intensity is observed when the CW laser is applied[26,42]. This effect is independent of laser polarization, we thus attribute the shift to charge screening from the large number of carriers generated in the surrounding material by the CW laser as in previous studies[26,42]. A similar blue shift is expected for the $X \to XX$ transition; hence Δ_{CW} is dependent on the incident CW laser intensity (I) according to:

$$\Delta_{CW}(I) = \Delta_{CW}\vert_{I=0} - kI/\hbar, \tag{S6}$$

where k is a fitting parameter. Fig. 5(b) in the main paper shows δ_{FS} vs. the CW laser intensity measured at $E = 60$ kV cm^{-1} and the fits according to Eq. S4. The parameters used in these fits are shown in Table S1.

Knowing how the FSS depends on the CW laser intensity, we now discuss the fidelity of the hole spin initialization vs. the CW laser intensity. To demonstrate the increase of the hole spin fidelity by reducing the FSS using OSE, the hole spin fidelity was measured as a function of the CW laser intensity [see Fig. 5(c) in the main paper]. This data can be well reproduced by including Eq. S4 in Eq. 2 in the main paper:

$$F = 1 - \frac{1}{2}\left[\frac{(\delta_{FS}\vert_{I=0} + \Delta\omega)^2}{(\delta_{FS}\vert_{I=0} + \Delta\omega)^2 + (\Gamma_X - \Gamma_h)^2}\right], \tag{S7}$$

where Γ_X and Γ_h are the exciton and hole decay rate. Table S2 lists the parameters used in this fit. a is determined from the fit of the δ_{FS} vs. CW laser intensity measured at $E = 60$ kV cm^{-1}[see Fig. 5(b) in the main paper]. $\Gamma_X - \Gamma_h$ is determined from time-resolved pump-probe spectroscopy[33] as discussed in the main paper.